Energy Reports 8 (2022) 14382–14395

Contents lists available at ScienceDirect

Energy Reports

journal homepage: www.elsevier.com/locate/egyr

Research paper

Automatic detection of visual faults on photovoltaic modules using deep ensemble learning network

S. Naveen Venkatesh [a], B. Rebecca Jeyavadhanam [b], A.M. Moradi Sizkouhi [c], S.M. Esmailifar [d], M. Aghaei [e,f,*], V. Sugumaran [a,**]

[a] School of Mechanical Engineering, Vellore Institute of Technology, Chennai, India
[b] Department of Computer Applications, Faculty of Science and Humanities, SRM Institute of Science and Technology, Chennai, India
[c] Department of Electrical and Computer Engineering, Concordia University, Montréal, Canada
[d] School of Mechanical, Aerospace and Marine Engineering, Amirkabir University of Technology, Tehran, Iran
[e] Department of Ocean Operations and Civil Engineering, Norwegian University of Science and Technology (NTNU), Ålesund, Norway
[f] Department of Sustainable Systems Engineering (INATECH), University of Freiburg, Freiburg, Germany

ARTICLE INFO

Article history:
Received 18 June 2022
Received in revised form 1 October 2022
Accepted 26 October 2022
Available online xxxx

Keywords:
Photovoltaic modules
Autonomous fault detection
Deep neural network
Ensemble learning
Random forest
Unmanned aerial vehicle

ABSTRACT

The present study proposes an ensemble-based deep neural network (DNN) model for autonomous detection of visual faults such as glass breakage, burn marks, snail trail, and discoloration, delamination on various photovoltaic modules (PVM). The proposed technique utilizes an image dataset captured by RGB (Red, Green, Blue) camera mounted on an unmanned aerial vehicle (UAV). In the first step, the images are preprocessed by deriving spatial and frequency domain features, such as discrete wavelet transform (DWT), texture, grey level co-occurrence matrix (GLCM), fast Fourier transform (FFT), and grey level difference method (GLDM). The processed images are inserted as input in the proposed ensemble-based deep neural network (DNN) model in order to detect any visual faults on the photovoltaic modules (PVM). The performance of the proposed model is evaluated through classification accuracy, receiver operating characteristic (ROC) curve, and confusion matrix. The results demonstrate that the proposed ensemble-based deep neural network (DNN) model, along with the random forest classifier, achieved a classification accuracy of 99.68% for detecting visual faults on the PV modules. To verify the performance and robustness of the proposed model, we compare our model's results to those of various classification approaches described in the literature. The suggested approach is compatible with the commercial unmanned aerial vehicle (UAV) embedded flight management system for fault detection.

1. Introduction

The global demand for electricity has expanded tremendously as a result of technical breakthroughs, population explosions, and scientific advancements. Currently, fossil fuels such as coal, oil, and natural gas account for 79.7 percent of the energy used to produce electricity (D'Adamo et al., 2020). Extensive use of fossil fuels has hastened the depletion of natural reserves of coal, oil, and natural gas, resulting in their exhaustion within a few decades. Extensive use of fossil fuels has hastened the depletion of natural reserves of coal, oil, and natural gas, resulting in their exhaustion within a few decades. Furthermore, the usage of fossil fuels leads to greenhouse gas emissions that aid in global warming and climatic changes (Perveen et al., 2020). As a result of the rising energy demand and environmental crisis, renewable energy sources are adopted as an alternative to fossil fuels in electricity production. Studies reveal that 27.3% of the total electricity production is constituted by renewable energy sources, among which solar-based photovoltaic (PV) power production contributes around 2.8%. Solar-based power generation is the second leading contributor to renewable power generation (Venkatesh and Sugumaran, 2021). Solar energy generation has drawn more capitalists and investors due to its widespread and year-round availability. The total global photovoltaic module (PVM) installations are projected to reach 440 gigawatts (GW) by 2022, according to several reports and publications (Tang et al., 2020). Additionally, the drop-in PVM prices (99% within the last three decades) has attracted several investors and capitalists to adopt PVM power generation (Naveen Venkatesh and Sugumaran, 2022).

* Corresponding author at: Department of Ocean Operations and Civil Engineering, Norwegian University of Science and Technology (NTNU), Ålesund, Norway.
** Corresponding author.
E-mail addresses: mohammadreza.aghaei@ntnu.no (M. Aghaei), sugumaran.v@vit.ac.in (V. Sugumaran).

https://doi.org/10.1016/j.egyr.2022.10.427

Apart from all the highlights, PVM power generation confronts the following challenges: (i) output power degradation, (ii) different types of faults, (iii) reliability of modules, (iv) varying operational environment, (v) high installation cost, (vi) requirement of large geographical regions (Pillai and Rajasekar 2018). PVM is placed outdoors under changing climatic conditions causing fault occurrences like snail trail, glass breakage, delamination, discoloration, and burn marks (Aghaei et al., 2022; Kettle et al., 2022). These faults in PVM can hinder the life span, reliability, and power output, raising severe concerns for safe operation. Recent reports infer that faults account for 18.9 percent of yearly output power loss (Madeti and Singh, 2018). Additionally, a study on degradation of various types of photovoltaic module states that the annual power degradation in monocrystalline, polycrystalline and amorphous silicon modules were estimated to be 1.23%, 1.43% and 1.67% per year respectively. Furthermore, the estimated lifetime of the modules ranges between 13–16 years (Aboagye et al., 2021). In this context, an accurate and on-time fault diagnosis can help increase the power output, useful lifespan, and reliability of PVM, thereby ensuring safe operation (Moradi Sizkouhi et al., 2021). The primary purpose of fault diagnosis is to discover and categorize defects so that the appropriate preventative action may be taken for a given scenario. Conventionally, a trained professional carried out PVM fault diagnosis through visual inspection. However, such inspections require more human resources, consume more time, and are not feasible for large-scale installations. Nowadays, more advanced non-destructive inspections on PVM like electroluminescence imaging, photoluminescence imaging, thermographic assessments, and electrical measurements are performed to diagnose PVM faults (S and Sugumaran, 2020). String data analysis was also utilized in assessing shading fault condition in PVM (Zsiborács et al., 2021). Hong et al. classified photovoltaic fault detection methods into two categories namely, (i) visual and thermal methods — lock in thermography, visual inspection, infrared thermography, electroluminescence imaging etc., and (ii) electrical based methods — IV characteristics, power loss analysis, artificial intelligence techniques etc (Hong and Pula, 2022).

Currently, unmanned aerial vehicles (UAVs) have been employed extensively to diagnose a non-destructive fault on PVM (Sizkouhi et al., 2019). Advancements in UAV technologies have spread their application over different fields like photography, search & rescue, large-scale inspections, freight transport, surveillance, and disaster relief. As discussed in the following papers, the key takeaways of employing UAV technology are time consumption reduction, human interference minimization, and its non-destructive nature. A contactless and non-destructive inspection was performed on PVM using a UAV equipped with thermal cameras (Grimaccia et al., 2018; Kirsten Vidal de Oliveira et al., 2020; Vidal de Oliveira et al., 2019). Poor thermal image resolution and higher UAV speed have confined the system from detecting hotspots at high temperatures. Hot spots in a PVM represent the presence of faults like micro-cracks, solder bond failure, short circuits, corrosion, and partial shading. Detecting the fault mentioned above can be challenging since thermal images are composed of thermal radiation information represented in pseudocolor images (Grimaccia et al., 2017). Given the drawbacks mentioned above, thermal imaging cameras are being replaced with high-resolution digital cameras to identify small faults with high precision. Digital cameras installed on UAVs acquire true-color images from PVM that aid in detecting visible faults like snail trail, glass breakage, delamination, discoloration, and burn marks. Several authors have adopted various image processing methods such as correlated texture feature extraction (Li et al., 2017), aerial triangulation (Tsanakas et al., 2017), image mosaicing (Leva et al., 2015), and edge detection (Tsanakas et al., 2015) to detect faults in PVM. However, the performance of the above-mentioned techniques relies highly upon the resolution of the images acquired using a UAV. Additionally, several other factors like vehicle vibration, wind speed, haze, and reflection can deteriorate the acquired UAV image resolution.

A convolutional neural network (CNN) is a common technique that delivers precise classification results while using low-resolution images in various fault diagnosis applications (Sizkouhi et al., 2022). Deep learning architectures are formulated by stacking CNN layers together that can be utilized to extract, select and classify features of an image in machine vision applications (Lu et al., 2019). Involving deep learning techniques in fault diagnosis has proved to outplay the classification performance displayed by traditional methods. Several researchers have adopted CNN in literature for diagnosing PVM faults, which are discussed as follows. A fault pattern recognition algorithm was designed using deep learning to detect five PVM test conditions, namely, encapsulant discoloration, glass breakage, snail trails, encapsulant delamination, and dust shading. The authors utilized a CNN network depicting the VGG16 network model in which a support vector machines classifier replaced the softmax layer to distinguish between PVM faults (Li et al., 2018). Cascading autoencoders (CASAE) were adopted to detect surface-level defects on a metal surface through segmentation and localization of defect regions. The defect regions were classified into classes like dust occurrence, damage spot, and glue mark using a compact CNN (Tao et al., 2018). Wang et al. attempted to classify PVM condition using features like perimeter, ratio of contour to outer rectangle, contour area and aspect ratio extracted from thermal images. U-net architecture was applied to segment the mask regions in thermal images of photovoltaic modules to identify fault occurrences (Wang et al., 2022). Akram et al. used electroluminescence images to locate flaws using CNN automatically. The authors used a publically available dataset consisting of electroluminescence images and attained a classification accuracy of 93.02% (Akram et al., 2019). Li et al. carried out fault diagnosis of PVM available in PV farms constructed on a large scale with a deep learning approach. Features from PVM images were extracted and further classified using a deep learning technique (Li et al., 2019). U – net architecture was adopted by Wang et al. to monitor photovoltaic panels using infrared images acquired from drones. Segmentation and masking were performed on the panels to determine the condition (Wang et al., 2022). Additionally, hotspots in a photovoltaic panel were detected using YOLOv5 network by Tianyi Sun et al. The model produced a classification accuracy of 98.6% over infrared images (Sun et al., 2022).

Numerous research has utilized various machine learning (ML) techniques to classify PVM problems, as will be mentioned here. Three different fault types were classified using the Naïve Bayes algorithm from thermal images of PVM that achieved 94.1% classification accuracy (Niazi et al., 2019). Bouraiou et al. and Harrou et al. employed SVM to classify fault occurrences in a PVM (Bouraiou et al., 2018; Harrou et al., 2019). String level faults in a photovoltaic array were identified with a classification accuracy of 98.7% using the k-nearest neighbor (kNN) algorithm by Madeti et al. (Madeti and Singh, 2018). In another investigation, visual faults in PVM were discriminated accurately using kNN classifiers (Naveen Venkatesh and Sugumaran, 2022). A combined approach of CNN and random forest classification was attempted by Ying et al. to classify cell-level faults in a PVM (Ying et al., 2019). Electroluminescence images of PV cells were fed as input to CNN, where image features were extracted and supplied to a random forest classifier for further process. Similarly, Naveen et al. adopted random forest algorithms to classify faults in a PVM (Sridharan and Sugumaran, 2021). Additionally, Chen et al. attempted an intelligent technique to diagnose array

faults involving an ensemble learning random forest algorithm. An adaptive neuro fuzzy interference system was used to detect faults in photovoltaic system. Subtractive clustering and grid partition strategies were used to train the fuzzy system (Abbas and Zhang, 2021). It can be inferred that ML algorithms can produce accurate results while working with numerical data, consuming less training time and computational efforts with versatile applications (Chen et al., 2018).

In recent times, CNN-based techniques have evolved to a great extent that they have been used in a wide range of applications. The significant advantage of using CNN models is that the model architecture can be constructed from scratch or adapted from public repositories (pre-trained network version). Studies reveal that pre-trained networks outperform models created from scratch due to the following reasons: (i) pre-trained models are accomplished with million images from different classes, (ii) the model weights are available in public repositories and accessible, (iii) the model can be modified based on user requirement (transfer learning) and (iv) compatible with any application producing accurate results. AlexNet (Krizhevsky et al., 2017) and VGG16 (Krishnaswamy Rangarajan and Purushothaman, 2020) are the most widely used networks for image classification tasks among all the pre-trained networks available. Several literature studies representing the pre-trained networks application are described as follows. Pierdicca et al. carried out an automatic PV cell fault detection using thermal images. The defects in the PV cells were identified and detected using a deep CNN replicating VGG16 architecture (Pierdicca et al., 2018). Pre-trained AlexNet was implemented by Aziz et al. to identify faults in PV arrays.

Recently, CNN has displayed exceptional performance in extracting features even on low-resolution images due to their self-learning ability and high compatibility (Aziz et al., 2020). The performance of deep learning models to produce accurate results depends highly on the training method and the volume of the dataset. Therefore, a massive volume of data is needed to train a CNN model in order to learn all the image features appropriately. However, acquiring vast data for a specific problem is challenging. Data augmentation is considered the best solution to confront this problem. Data augmentation is the process of artificially increasing a limited dataset in order to obtain adequate information for training purposes. Numerous literature has discussed using a generative adversarial network (GAN) to augment the acquired dataset (Luo et al., 2019). However, such techniques comprise numerous convolutional layers stacked together, thereby consuming more training time and hardware requirements.

In general, CNN has achieved great performances in fault diagnosis. However, CNN utilizes local features to perform classification tasks. During dimensionality reduction, the pooling layers can lose vital information and deplete the relationship between the whole image and a part of the image. The fusion technique is implemented to overcome the constraints of CNN feature extraction. Because the strengths of individual features may be combined to create more accurate findings, this technique has attracted the attention of researchers. Haidong Shao et al. diagnosed faults in rotating machinery using an enhanced deep feature fusion strategy (Shao et al., 2017). Similarly, Liang et al. attempted to diagnose roller-bearing faults with the aid of feature fusion using parallel CNN. The study fused time and frequency domain features to enhance the feature information (Liang et al., 2021). Gear fault diagnosis was carried out by Pan et al. using an extreme learning machine and feature fusion optimization (Pan et al., 2021). Individual features were traditionally extracted, and fault diagnosis was carried out on PVM images. However, feature fusion strategies (on features retrieved from image data) have not been explored, paving the way for more experimentation.

Ensemble-based techniques are now gaining popularity among researchers since the weaknesses of individual techniques are eliminated, and their strengths are integrated to give more precise results. Ensemble approaches have shown to be beneficial, as demonstrated by the research reviewed below. Eskandari et al. attempted an ensemble model combining kNN, SVM, and Naïve Bayes to detect line faults in a PVM (Eskandari et al., 2020a). Justin et al. attempted a stacking and bagging-based ensemble approach to detect PV faults. Stacking-based ensemble produced a classification accuracy of 94%, while bagging delivered 79.5% accuracy (De Guia et al., 2020). A combined ensemble model of SVM, kNN, and decision tree was employed by Dhibi et al. to classify string-level PVM faults. Traditionally, ensemble learning models were applied to numerical data retrieved from I–V characteristics measured at PV plants or through various analytical models (Dhibi et al., 2021). However, ensemble-based techniques using features retrieved from image data have not been explored thoroughly, paving the way for more experimentation. Table 1 represents a summary of the works carried out in diagnosing PVM faults.

The following observations were made based on the literature mentioned above.

(i) Most of the literature employs electroluminescence or thermal images for detecting faults in PVM. A few studies attempted to adopt true-color or RGB images.
(ii) Electroluminescence images were confined only to detecting cell cracks, while thermographic assessments were limited to detecting hotspots. Also, only a limited number of faults were identified and diagnosed in many studies.
(iii) There exists a vital challenge in acquiring image datasets due to the non-availability and scarcity of datasets in public depositories
(iv) Data augmentation was carried out using GAN, which contains multiple convolutional layers resulting in increased computational time and hardware requirements. Adopting data augmentation techniques without GAN can help eliminate the challenges mentioned above.
(v) Features extracted from CNN have been utilized to perform PVM fault diagnosis. However, feature fusion strategies were less explored.
(vi) Ensemble-based techniques were applied to the dataset retrieved from I-V characteristics measured at PV plants. However, ensemble-based techniques using features retrieved from the image dataset have not been explored thoroughly.

The challenges above imply a need to develop an intelligent and effective fault diagnosis technique. Deep learning algorithms display exceptional feature extraction properties, while machine learning algorithms can produce accurate results on numerical data. The present study recommends using various segmentation techniques that contribute toward the detection of PVM faults with the aid of PVM aerial images and machine learning classifiers. Fig. 1 represents the overall workflow proposed in this article. The contributions of the paper are summarized as follows.

1. An ensemble-based deep neural network (DNN) model is proposed to identify the faults on PV modules such as glass breakage, burn marks, snail trail, discoloration, and delamination.
2. PVM images features are derived from the spatial and frequency domain features, including discrete wavelet transform (DWT), texture, grey level co-occurrence matrix (GLCM), fast Fourier transform (FFT), and grey level difference method (GLDM), and fused inside the ensemble-based DNN model to perform PVM fault diagnosis.
3. The feature extraction process and the ensemble-based DNN model algorithms are developed to exhibit the impact of feature fusion on classification.

Table 1
Related works on PVM fault diagnosis.

Technique adopted	Dataset utilized	Reference
CNN based on U-Net architecture	Thermal images	(Wang et al., 2022)
Deep CNN replicating VGG16		(Pierdicca et al., 2018)
Convolutional neural network	Electroluminescence images	(Akram et al., 2019)
CNN with Random Forest		(Ying et al., 2019)
Custom CNN		(Li et al., 2019)
CNN with decision tree algorithms	RGB images	(Sridharan and Sugumaran, 2021)
CNN with lazy algorithms		(Naveen Venkatesh and Sugumaran, 2022)
Adaptive neuro fuzzy interference system	I-V characteristics	(Abbas and Zhang, 2021)
Pre-trained AlexNet		(Aziz et al., 2020)
Ensemble model combining kNN, SVM, and Naïve Bayes		(Eskandari et al., 2020a)
Stacking based ensemble		(De Guia et al., 2020)

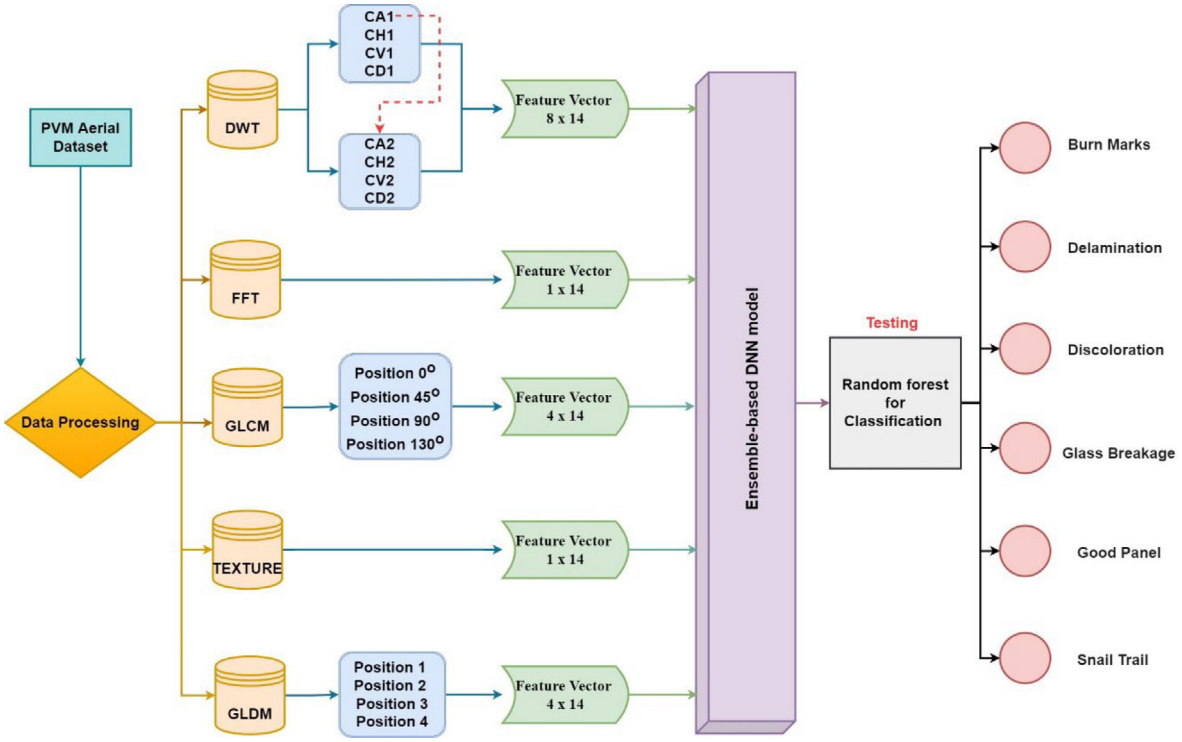

Fig. 1. The overall workflow of the proposed ensemble-based DNN model to diagnose PVM test conditions.

4. Performance comparison is carried out with other techniques proposed in the literature to show the proposed method's capability.

The overall manuscript is outlined as follows. Section 2 describes the experimental studies involving the experimental setup, experimental procedure, and a brief description of various visual faults in PVM. In Section 3, the feature extraction process using various segmentation algorithms like discrete wavelet transform (DWT), texture, grey level co-occurrence matrix (GLCM), fast Fourier transform (FFT), and grey level difference method (GLDM) are explained, followed by short notes of the random forest algorithm in Section 4. The obtained experimental results are reported in Section 5, followed by the conclusion in Section 6.

2. Experimental process

The primary objective of the present study is to diagnose PVM test conditions as healthy or defective. If the diagnosed condition is defective, then the proposed technique aims at detecting the type of PVM fault. The current section describes the experimental setup adopted, the procedure involved in acquiring aerial images of PVM test conditions, and a brief description of various PVM faults.

2.1. Experimental setup

The experimental setup adopted in the study involves PVM (with healthy and fault conditions), a UAV equipped with a high-resolution digital camera, various sensors, on-board processors, and a ground control station (Niccolai et al., 2019). The modules utilized in the present study were manufactured by Udhaya semiconductors limited under operation. The images of PVM were acquired by DJI Mavic 2 Zoom UAV (see Table 2) under laboratory conditions. A trained professional held a remote controller to control the UAV operation. A digital RGB camera attached to the UAV was used for image acquisition. The captured images were stored on the storage system located at the ground station. The stored images were further processed and fed into the ensemble-based DNN model for feature extraction and classification. Pre-processing of images might not be mandatory during real-time operations since the results must be instantaneous. A total of six PVM test conditions (Five faulty and one healthy)

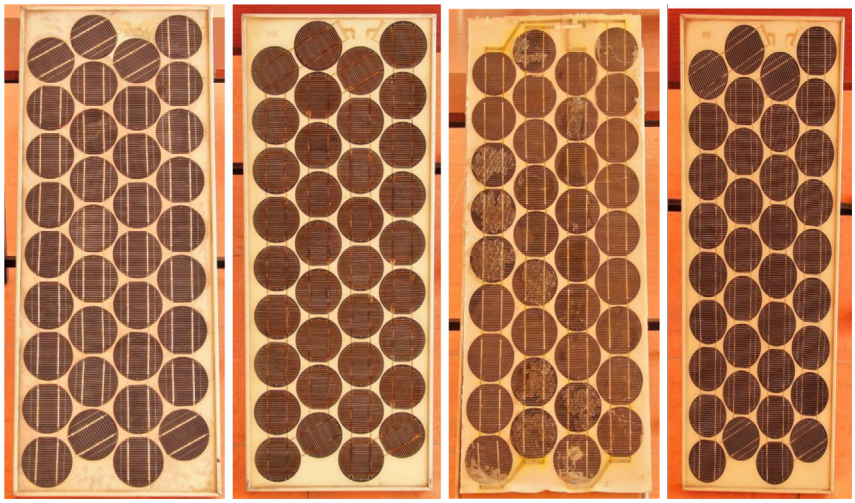

Fig. 2. PVM sample images.

Table 2
DJI Mavic 2 Zoom specification.

Parameter	Value
Weight	1.6 kg
Length	322 mm
Image sensor size	6.18 mm × 4.50 mm
Operational range	5 km
Propulsion	Electric power
Flight endurance	0.28–0.70 h
Mission altitude	20–30 m
Wingspan	0.354 m
Cruise speed	10–20 m/s
Maximum resolution	4000 × 3000

Table 3
Detailed specification of PVM.

Parameter	Value
Number of cells	36
Efficiency	9%–10%
Maximum power point current (I_{mpp})	2.1
Maximum power	36 W
Maximum power point voltage (V_{mpp})	17 V
Voltage (V_{oc})	20.6 V
Dimensions	(1011 × 435 × 36) mm
Weight	3.5 kg
Current (I_{sc})	2.25 A
Type	Monocrystalline
Model name	USP-36

*All values measured at standard test conditions of 25 °C, 1000 W/m^2 irradiance and AM 1.5 spectrum.

were utilized during image data acquisition. Table 3 represents the detailed specifications of PVM adopted in the study.

During data acquisition, the UAV was operated between 1–5 meters above the PVM for data collection. The UAV was operated in two sessions (each lasting about 14 min) to acquire PVM images. Every test condition of PVM, namely, snail trail, glass breakage, delamination, discoloration, healthy module, and burn marks, was placed at various positions inside the laboratory for image data acquisition. One hundred images were collected for every test condition for each PVM condition. A sample of images captured is depicted in Fig. 2.

2.2. Experimental procedure

The experiment was carried out in four different stages: (i) data acquisition, (ii) feature extraction using various image segmentation techniques, (iii) fusion of features using an ensemble-based DNN model and (iv) features classification using random forest classifiers. Initially, 600 images (100 images for every class) were attained and categorized into different classes. Dataset preparation is a crucial step in dealing with a deep learning problem. A primary solution is to take advantage of data augmentation techniques. In this experimental research, 3150 images are prepared, through which 525 images are allocated to each class. Table 4 represents the image transformations applied to the image dataset for data augmentation. A balanced dataset is obtained for further feature extraction. Finally, the extracted features were fused using the ensemble-based DNN model equipped with a random forest classifier to perform classification.

2.3. Visible faults in PVM

Faults in a PVM can be induced due to extreme environmental uncertainties, thermal stresses and changing climatic conditions. The occurrence of faults in PVM can significantly affect the performance, life span and reliability of PV modules. Table 5 describes the most commonly occurring visual faults, while a pictorial representation of such faults is provided in Fig. 3.

3. Feature extraction using advanced segmentation techniques

The process involving a reduction in variables to describe and understand large volumes of data is termed feature extraction. Before feature extraction, the acquired PVM aerial images were resized to a uniform size of 512 × 512 pixels. Additionally, the color space of the images is converted into grayscale and provided as input of size 512 × 512×1 for the application of segmentation techniques.

The present study adopts several well-established image segmentation methods like Fast Fourier Transforms (FFT), Grey Level Difference Method (GLDM), Discrete Wavelet Transforms (DWT), Texture and Grey Level Co-Occurrence Matrix (GLCM) to extract images features based on the statistical features derived. A total of 252 features were formulated (combined number of features) from all the segmentation techniques adopted. The statistical features computed in the present study are provided as follows:

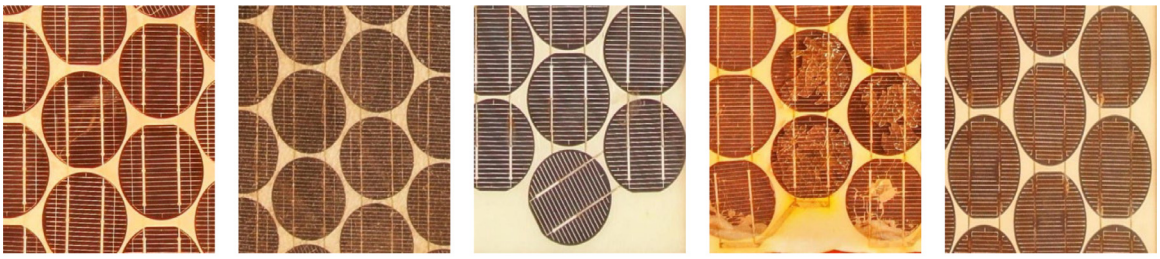

(a) Snail trail (b) Glass breakage (c) Delamination (d) Discoloration (e) Burn marks

Fig. 3. Various visual faults in PVM.

Algorithm 1. Resizing PVM aerial images.

Resizing
Input (U) = PVM image U (a,b,c,d,e,f) $_{(a,b,c,d,e,f)}$ ε $_{(1,2,3,.....n)^3}$, a = b = c = d = e = f
Output (V)- Image output V (a,b,c,d,e,f) $_{(a,b,c,d,e,f)}$ ε $_{(1,2,3,.....n)^3}$, a = b = c = d = e = f
Begin
for each PVM image input U do
for {a, b, c, d, e, f} = 1 to n do,
Convert PVM image input U to grey scale along with resize to 512×512
Application of normalisation (min-max) and return grey scale image ouput (V)
end for
end for

Algorithm 2. Feature extraction from various segmentation techniques

Feature extraction
Input (V) : Input resized image V (a,b,c,d,e,f) $_{(a,b,c,d,e,f)}$ ε $_{(1,2,3,.....n)^3}$, a = b = c = d = e = f
Output : Ensemble-based DNN
Begin
for each grey image V do
for (a,b,c,d,e,f) = 1 to n do
if file ← a, Then
label ← 0 elif file ← b label ← 1 elif ← c label ← 2 elif ← d label ← 3 elif ← e label ← 4 elif ← f label ← 5 end if
end for
end for
Y ← { calculate input image features V (Density, Area, Skewness, Std_Density, Energy, Kurtosis, Entropy, Max, Median, Min, Mean Absolute Deviation, RMS, Uniformity and Range)}
GLCM(GC) ← calculate Y on image input V in four orientation GLDM (GD) ← calculate Y on image input V in four orientation WT (D_1) ← calculate Y on image input, V DWT (D_2) ← calculate Y on image input, V DT ← D_1+ D_2 FFT (FT) in eq.(1) ← calculate Y on image input,V Textural, (TX) ← calculate Y on image input, V
Ensemble-based DNN ← $\sum_{i=1}^{n}$ {GC, GD, DT, FT, TX} ε V (Total Y = 252)
Model Save

Table 4
Basic image transforms used for PVM dataset augmentation.

Transform operation	Noise	Warp	Rotation (Clockwise, Anticlockwise)	Flip (Horizontal, Vertical)	Blur
Value	Random	40	0°–180°	90°	Gaussian

Table 5
Visual fault occurrence in photovoltaic modules.

S.No	Visual faults in PVM	Reason for the occurrence of a fault	Effect on modules
1	Delamination (Sánchez-Friera et al., 2011)	Adhesion loss between back cover, encapsulant and glass	Moisture invasion leading to corrosion
2	Glass breakage (Chandel et al., 2015)	Physical damage during transport and installation, Thermal Stresses	Lower Irradiance, Corrosion and Moisture invasion
3	Snail trail (Dolara et al., 2016)	Stress acting upon micro-cracks along edges	Quicker Degradation
4	Discoloration (Han et al., 2018)	Elevated exposure to ultraviolet radiation, heat and humidity	Physical color change of modules (Browning or Yellowing), Power loss
5	Burn marks (Köntges et al., 2014)	Solder bond failure, ribbon breakage and localized heating	Safety hazards and performance degradation

Algorithm 3. The training algorithm of the ensemble-based DNN model.

Ensemble-based DNN Training
Input: Ensemble-based DNN, classifier = Random Forest, train test split ratio = 80% : 20%, number of trees = 100
Output: Performance index, Plot, Confusion Matrix
Begin
for ensemble-based model input do m = concatenate{(a(Y), b(Y), c(Y), d(Y), e(Y), f(Y))} ε (1, 2, 3, …..n)^3 (input) n = concatenate {(a(Y), b(Y), c(Y), d(Y), e(Y), f(Y))} ε (1, 2, 3, …..n)^3 (target labels)
end for

area, density, standard density, skewness, kurtosis, energy, entropy, maximum, mean absolute deviation, median, minimum, range, root mean square and uniformity. The image segmentation techniques delivered 252 features combined (14 FFT, 56 GLCM, 56 GLDM, 14 texture, and 112 DWT). The algorithms involved in resizing the images, the feature extraction and the training of the ensemble-based DNN model are presented in Algorithms 1, 2 and 3, respectively. A brief description of the adopted segmentation techniques is provided below.

3.1. Grey level co-occurrence matrix (GLCM)

The grey level co-occurrence matrix is a second-order statistical process that investigates texture features based on the spatial relationship of pixels. The primary role of GLCM is to identify the frequency of pixels' combination appearance in a particular image for a given distance and direction. GLCM is generally computed in four directions and at different distances over which the texture features are highlighted. The measurement boundary during GLCM application is determined by adopting the middle value from various directions (Alvarenga et al., 2007). A grid-based system is adopted to identify the textural highlights in horizontal, vertical, and diagonally up and down directions from specific distances. The GLCM segmentation of a sample PVM fault is represented in Fig. 4 with cell, module and GLCM dissimilarity in four positions. The co-occurrence matrix (R) displays different possible combinations of grey levels within an image where a and b (elements in various grey levels) are placed at a distance d (displacement vector) along with the direction e (one among eight orientations), R (a, b | d, e). However, only four probability orientation matrices are created since opposite directions

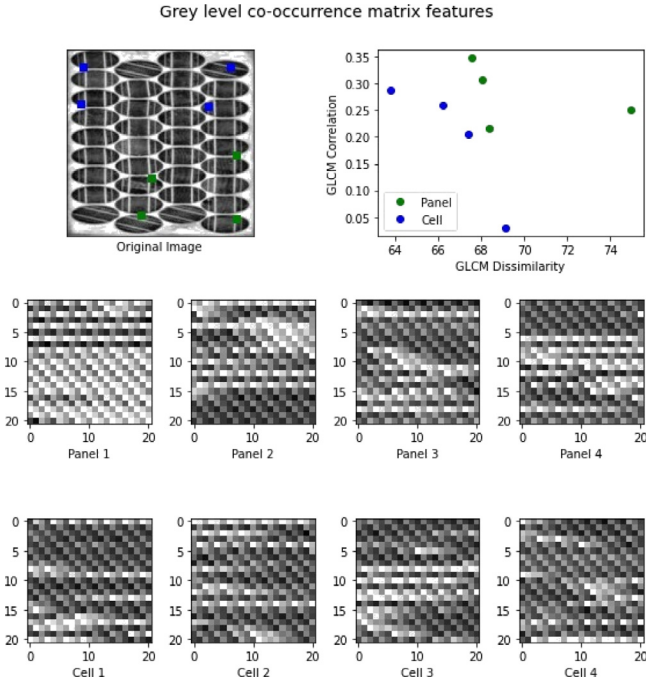

Fig. 4. Grey level co-occurrence matrix (GLCM) segmentation for a sample PVM aerial image.

are always ignored. The symmetric matrices are utilized in four directions, namely, 0°, 45°, 90° and 135°. A correlation texture

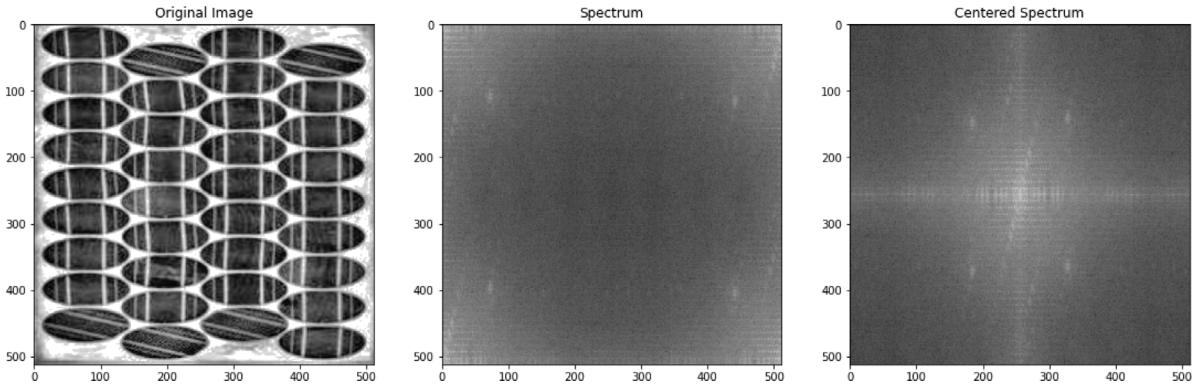

Fig. 5. Fast Fourier transformation (FFT) segmentation for a sample PVM aerial image.

function (T) was adopted to calculate the texture feature. Eq. (1) represents the GLCM feature extraction, while Eqs. (2), (3), (4) and (5) denote the parameters.

$$T = \sum_{a,b} \frac{(a-\delta_a)(b-\delta_b) R(a,b)}{\sigma_a \sigma_b} \tag{1}$$

$$\delta_a = \sum_{a,b} a.R(a,b) \tag{2}$$

$$\delta_b = \sum_{a,b} b.R(a,b) \tag{3}$$

$$\sigma_a = \sqrt{\sum_{a,b} (a-\delta_a)^2 .R(a,b)} \tag{4}$$

$$\sigma_b = \sqrt{\sum_{a,b} (b-\delta_b)^2 .R(a,b)} \tag{5}$$

3.2. Fast Fourier transforms (FFT)

Fast Fourier transform is a computer algorithm oriented towards the computation of discrete Fourier transform (DFT) for a sequence of variables or the inverse of DFT (IDFT). FFT is widely used for calculating various frequency elements from different time-domain signals and is capable of reconstructing the signals through a set of frequency values. The primary role of FFT is to transform a digital signal (d) of range (R) from the time domain into the frequency domain (F) depending upon the parameter value (Márquez and Papaelias, 2019). During FFT, the frequency spectrum vector is divided into several frequency levels to automate the selection of sensitive frequency toward fault occurrence that is considered. Furthermore, the mean of every frequency range is considered the sensitive element of each condition. FFT was adopted to calculate 14 statistical features for all the images in this experimental research. Eq. (6) represents the working of FFT, while a sample observation of FFT imposed on a PVM image is presented in Fig. 5, in which the difference between the spectrum and centered spectrum can be observed.

$$R[k] = \sum_{i=0}^{F-1} d(i) W_F^{ik}, W_F = e^{-\frac{2\pi i}{F}}, for\ k = 0, 1, 2 \ldots \tag{6}$$

3.3. Discrete wavelet transforms (DWT)

Discrete wavelet transforms (DWTs) are a characteristic representation of a non-redundant tested continuous wavelet transform (CWT). The wavelet transforms are used to represent a discrete-time series arrangement in the form of numerous coefficients of wavelets. Such wavelet coefficients are examined with the aid of CWT to achieve a bio-orthogonal or symmetrical region. Non-redundancy of the signal to be portrayed is guaranteed while utilizing symmetrical regions. In general, symmetrical representations can provide direct calculations for the remaking and disintegration of signals. However, calculating the value of productive wavelets consumes more computational efforts that are not oriented towards actualizing an instantaneous Fourier transform (Bentley and McDonnell, 1994). In this paper, wavelets are described based on the channel bank idea in which the wavelets are characterized as two finite impulse response channels with N coefficients. Among the two channels, one is considered a high pass channel while the other is considered a low pass channel (capable of cutting off the inspection recurrence). The characterization of a wavelet transform can be performed using the channels mentioned above through recursive application. Initially, the high pass $f_1(m)$ and low pass $f_2(m)$ elements are derived from the channels by applying the input time arrangement as provided in (7) and (8).

$$f_1(m) = \sum_{i=0}^{N-1} x_i f(m-i) \tag{7}$$

$$f_2(m) = \sum_{i=0}^{N-1} y_i f(m-i) \tag{8}$$

Where x_i and y_i are the low and high pass channel coefficients. Additionally, one can build a high pass channel based on the low pass channel through a rotating flip plan (9).

$$y_i = (-1)^i e_{N-1} \tag{9}$$

The present experimental study adopted a sequential two-way operation to estimate the coefficients like CH1, CA1, CD1 and CV1 and other coefficients formulated using CA1, namely, CH2, CA2, CD2 and CV2, depending upon the 14 statistical features. Fig. 6 represents the wavelet transforms applied to a sample PVM image.

3.4. Texture analysis and Grey level difference method (GLDM)

Texture has proved to be a necessary and sufficient feature that helps handle several computer vision applications. Works of literature involving texture analysis revealed that the necessary parameters for image refining revolve around union, division and order. Image recovery, investigation of clinical images and aeronautical & satellite image examinations are various applications of texture analysis (Manjunath et al., 2005). The present section exhibits a method to portray texture features based on multi-band image disintegration that can be applied for object recognition, characterization, image recovery and division. On

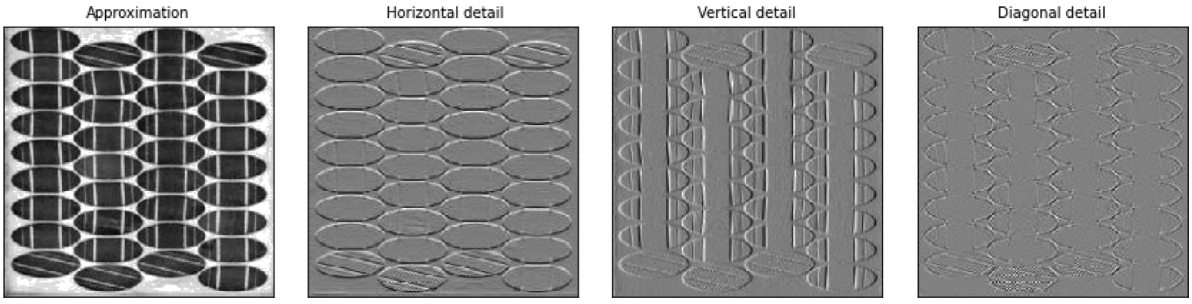

Fig. 6. Wavelet transforms (DWT) segmentation for a sample PVM aerial image.

the other hand, the grey-level difference method calculates the statistical grey level difference between thickness capabilities in a grey image. Additionally, the density among the image's most significant and least significant regions can be calculated based on the contrast adjustments. Homogeneity in an image is proportional to the angular second moment, considered the measurement metric. Accordingly, 14 statistical features were calculated for four spatial regions at a distance of $s = 8$ from the neighboring pixels (m, n) and reference points for all images in a dataset. In (10) the GLCM distance calculation is represented for every input image j for the corresponding output image k.

$$k(m,n) = |j(m,n) - j(m,n+s)| \tag{10}$$

4. Classification using random forest

Random forest is an ensemble technique that applies a supervised learning strategy to solve regression and classification problems. As the name suggests, the forest is a term used to denote a collection of trees, and a more significant number of trees deliver a more vigorous forest. Random forest works by adopting multiple decision trees accompanied by the information gain obtained from the trees (Chen et al., 2018; Ying et al., 2019). Subsequently, the decision trees' output is forecasted so that the best results are identified through voting strategy. In general, a group's decisions are superior to the individual decisions delivered by the tree since the model avoids overfitting, thereby averaging the outcome. Fig. 7 represents the random forest algorithm operation. The random forest has exhibited exceptional classification performance over other machine learning classifiers due to its versatile nature, easy adaptability, high precision and ensemble strategy. Hence, a trained random forest was adopted in this study to perform the PVM test condition calculation. The hyperparameters for the random forest network *i.e.,* the number of trees, were set as 100 to perform batch predictions. The random forest works on the following steps.

- Initially, random data samples are determined from the input dataset.
- Consequently, each data sample is represented in the form of decision trees. Additionally, the expected results can be obtained from every decision tree.
- Finally, a voting strategy has been applied to predict the possible outcomes.

4.1. Performance evaluation

The performance of a classifier can be evaluated using a confusion matrix. In a confusion matrix, the rows and columns represent the actual and predicted classes. The performance of the classifier is evaluated depending upon four factors, namely, true positive (TP), true negative (TN), false positive (FP) and false negative (FN) for every class. The present study evaluates the model performance based upon various performance metrics like accuracy and receiver operating characteristics (ROC). Accuracy is the measure of model performance that signifies the proportion of correctly classified samples that can be computed as given in Eq. (11) (Eskandari et al., 2020b).

$$Accuracy = \frac{TP + TF}{Total\ number\ of\ samples\ in\ a\ dataset} \tag{11}$$

The receiver operating characteristics (ROC) curve is a performance measure used to demonstrate the capability of a classification model. The curve is plotted against two major parameters: true positive rate (TPR) and false positive rate (FPR). In other words, TPR is termed as sensitivity while FPR is denoted as 1-specificity. Eqs. (12) and (13) represent the process of calculating TPR and FPR, respectively. ROC plots carry information about a corresponding sensitivity/specificity pair for every threshold passed, while the area under the curve (AUC) represents the model accuracy.

$$TPR = \frac{TP}{TP + FP} \tag{12}$$

$$FPR = \frac{FP}{FP + TN} \tag{13}$$

5. Results and discussion

The present study evaluates the performance of the developed ensemble-based DNN model in diagnosing various PVM test conditions using extracted features from advanced segmentation techniques. The PVM aerial images acquired from UAV are preprocessed before being fed into the ensemble-based DNN model. A total of 252 features consisting of 14 FFT, 56 GLCM, 56 GLDM, 14 texture, and 112 DWT features were derived and fused through an ensemble-based DNN model. A random forest classifier was coupled with an ensemble-based DNN model to classify PVM test conditions. The performance of the proposed ensemble-based DNN model, along with a comparison of state-of-the-art techniques, are discussed in this section.

5.1. Training and evaluation of the ensemble-based DNN model

The current study utilizes a designed ensemble-based DNN model and a random forest classifier to classify various PVM conditions, including snail trail, glass breakage, delamination, discoloration, healthy module, and burn marks. Features from advanced segmentation techniques like FFT, GLCM, GLDM, texture and DWT were extracted and fused through the concatenation layer in the ensemble-based DNN model. Random forest was used to classify the PVM test conditions from the concatenated features. Fig. 8 represents the overall performance of the ensemble-based DNN model involving the accuracy and loss curves. As shown in Fig. 8, the training and validation loss gradually decreases,

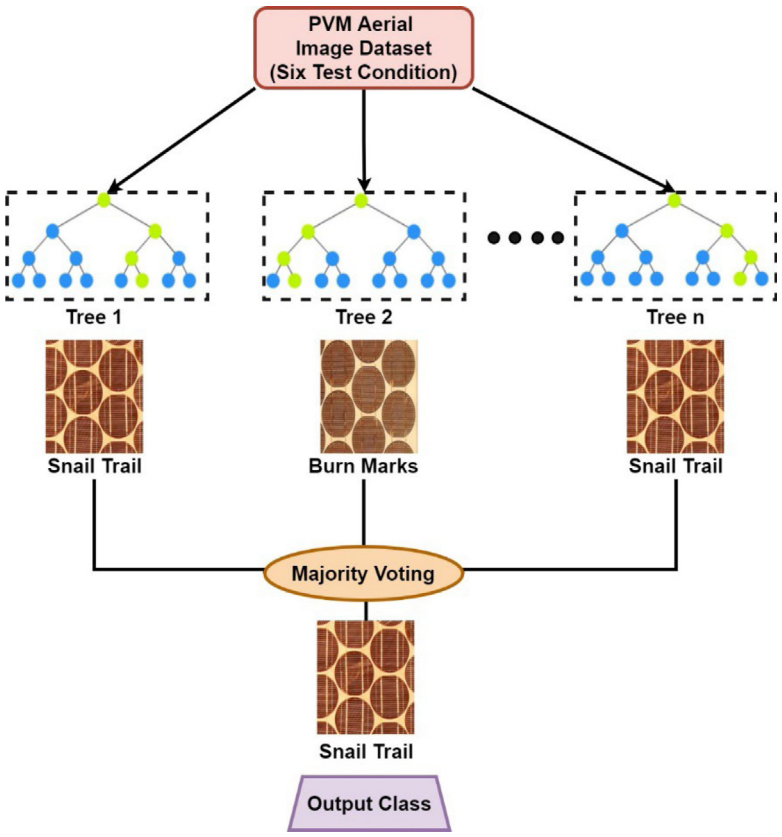

Fig. 7. The random forest algorithm illustration and classification.

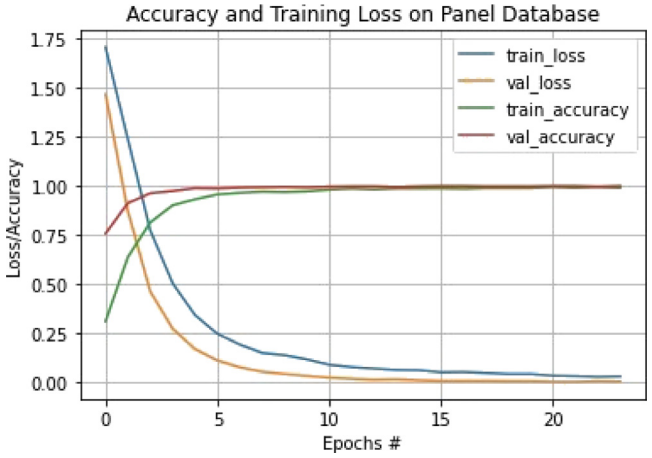

Fig. 8. The performance of the ensemble-based DNN model.

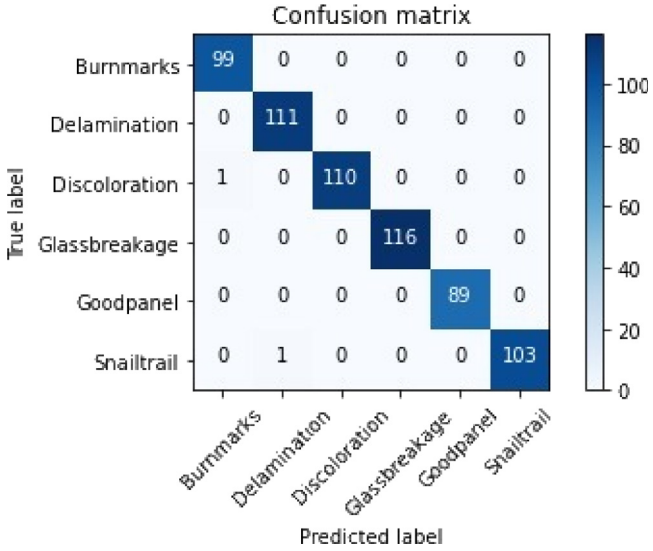

Fig. 9. The confusion matrix of the ensemble-based DNN model.

thereby improving the validation and training accuracies. The plot infers that the training process of the ensemble-based DNN model converges quickly on the applied PVM aerial dataset. Additionally, minimal loss values represent the evolution of a highly accurate model. The random selection of training and validation data has orchestrated the fine training of the model. Both the training and validation accuracy reaches a saturation (100%) after 10 epochs; thus, early stopping was implemented when further training resulted in no change of accuracy values.

To assess the performance of the model, a confusion matrix was designed to provide a clear insight into the prediction level of the trained model. In a confusion matrix, the rows and columns represent the actual and predicted test conditions of the PVM. Also, the shape of the confusion matrix is determined based on the number of test conditions adopted. The diagonal elements present in a confusion matrix represent the correctly classified instances, while the other elements represent misclassifications. Fig. 9 represents the confusion matrix obtained from the ensemble-based DNN model.

After dataset preparation, a total number of 3150 aerial images of PVM were collected, from which 2520 sample data was split for training, and 630 sample data was used for the test. Among the 630 test samples, the proposed ensemble-based DNN model

Table 6
Five-fold cross validation of the proposed ensemble model.

Fold 1 (%)	Fold 2 (%)	Fold 3 (%)	Fold 4 (%)	Fold 5 (%)	Overall accuracy (%)
98.09	99.96	100.00	99.72	99.12	99.38

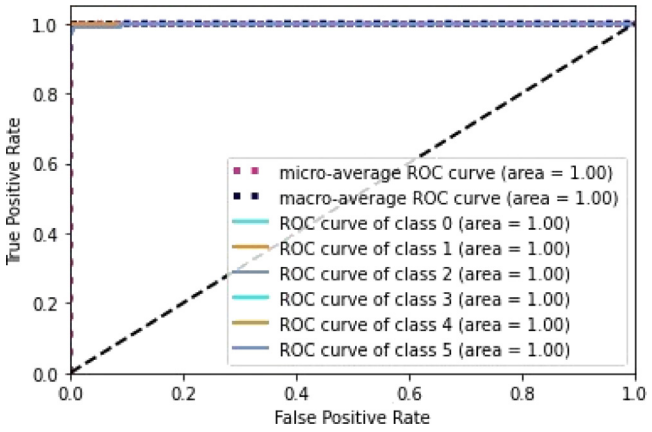

Fig. 10. ROC curve for the ensemble-based DNN model for PVM test conditions.

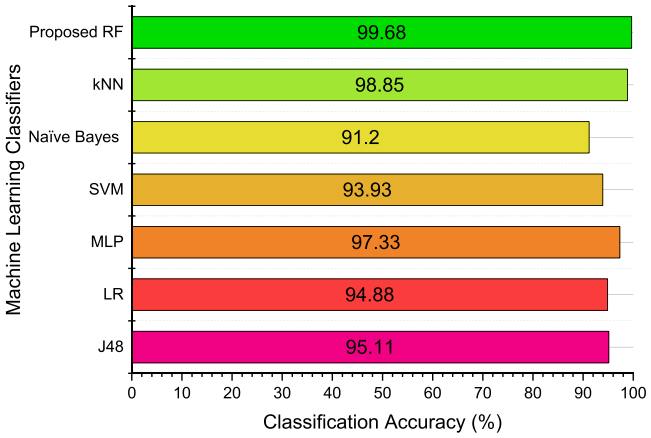

Fig. 11. Performance comparison of machine learning classifiers and proposed model.

achieved a high classification accuracy of 99.68% by producing only two misclassifications (1 sample each in discoloration and snail trail). To avoid the randomness in the obtained results a five-fold cross validation was carried out and the obtained results were presented in Table 6. The overall validation results display similar classification accuracy as obtained in the test set. The similarity in extracted features, noise interference and image resemblance are specific reasons for misclassification. The limited number of misclassifications infer that features are learned effectively and exhibit the feasibility of the proposed model. Feature fusion helps eliminate the drawbacks faced by individual features by compensating the weakness of one feature with the strength of other features that contribute toward classification. Fig. 10 represents the receiver operating curve (ROC) obtained for the ensemble-based DNN model.

5.2. Performance evaluation of the ensemble-based DNN model against pre-trained models

The proposed ensemble-based DNN model's performance is evaluated through a comparative analysis with various state-of-the-art pre-trained models. Deep learning models need a considerable amount of data for training. Pre-trained models are used to compare and analyze the performance of the proposed ensemble-based DNN model. Additionally, transfer learning is a helpful technique through which trained weights of another network are transferred to a designed model with minimal changes in the final few layers. Pre-trained models' weights are made available in public repositories for instrument transfer learning. In the field of computer vision, many pre-trained networks have been applied for performing classification tasks. Among the available pre-trained models, ResNet-50 (Wen et al., 2019) and VGG16 (Kim et al., 2017) have produced exceptional results in classification tasks and are widely adopted. This section presents a comparative study of pre-trained models' performance with the proposed ensemble-based DNN model, as represented in Table 7. As shown in Table 7, the proposed ensemble-based DNN model achieves an elevated performance than pre-trained and CNN models by providing an overall classification accuracy of 99.68%. The performance of the pre-trained and CNN models was hindered due to the high complexity in computation and model overfitting. Additionally, working with pre-trained networks require huge hardware requirements and robust systems to deliver results in minimal time, thereby increasing the capital cost. Overall, the proposed ensemble-based DNN model delivered better accuracy and consumed low computational efforts, thereby eradicating the need for sophisticated systems.

5.3. Performance evaluation of the ensemble-based DNN model against machine learning classifiers

Machine learning algorithms are widely used to perform classification and regression tasks. The present study compares the performance of a random forest aligned with the ensemble-based DNN model with various renowned machine learning classifiers like J48, Logistic Regression, Multilayer Perceptron, SVM, NB, and kNN (Naveen Venkatesh and Sugumaran, 2022). Fig. 11 represents the performance comparison of the ensemble-based DNN model with specified machine learning classifiers. As depicted in Fig. 11, it is evident that the proposed ensemble-based DNN model with random forest performs better in diagnosing PVM conditions than other machine learning classifiers. The kNN classifier has comparable performance to the proposed methodology with 98.85%. One can also observe that all the classifiers exhibit healthy classification accuracy (above 90%) for the developed aerial PVM dataset. However, since the computational cost of the proposed ensemble-based DNN model with a random forest classifier is affordable, it can be used in real-time applications. The comparative study performed in this section considered the features extracted from pre-trained models classified with machine learning classifiers and compared them with the proposed methodology.

5.4. Discussion

The present study adopts an ensemble based deep neural network to detect and classify PVM conditions with the aid of random forest classifier. Image features were extracted using various segmentation algorithms and fused together in the concatenation layer. Furthermore, the performance of the proposed model is assessed and compared with various state of the art techniques. The major findings from the study are discussed as follow:

Table 7
Performance comparison with various CNN models proposed in literature.

Methodology	Image type	Classification accuracy (%)	Reference
Isolated model	Infrared images	98.67	(Akram et al., 2020)
Custom CNN	Infrared images	99.00	(Manno et al., 2021)
Transfer learned model	Infrared images	99.23	(Akram et al., 2020)
Encoder Decoder	RGB images	93.00	(Moradi Sizkouhi et al., 2021)
Multiscale CNN	RGB images	97.32	(Korkmaz and Acikgoz, 2022)
Custom CNN	Infrared images	92.50	(Fonseca Alves et al., 2021)
Custom CNN	Time series graph	99.00	(Lu et al., 2019)
Custom CNN	Scalograms	73.53	(Aziz et al., 2020)
Pre trained VGG 16	RGB images	73.88	
Conventional pattern recognition	RGB images	74.50	(Li et al., 2019)
CNN based model	RGB images	97.00	
Pre trained Resnet 50	RGB images	90.00	(Bommes et al., 2021)
Proposed technique	**RGB images**	**99.68**	

- The image dataset of 3150 images was split with a train test split ratio of 80%–20% representing 2520 training images and 630 test images. Features from advanced segmentation techniques like FFT, GLCM, GLDM, texture and DWT were extracted and fused through the concatenation layer in the ensemble-based DNN model. The model was trained initially for 30 epochs with early stopping strategy that stops training when no further change in accuracy or loss was observed. The model displayed gradual rise and drop in accuracy and loss curves respectively. Smooth lines in the training process represents that the model has learnt the features effectively (Fig. 8). The confusion matrix in Fig. 9 represents the overall classification accuracy of the proposed model with 99.68%.
- Among the 630 test instances, one can observe that only 2 instances were misclassified representing the phenomenal performance of the proposed methodology. Also, ROC curves represented in Fig. 10 display values of 1 thereby providing a clear insight about the elevated performance of the proposed method.
- To establish the superiority of the proposed method, various state of the art techniques in CNN and machine learning were compared. Considering CNN based techniques, several pre-trained and CNN models exhibited in literature were compared with the proposed method. From Table 7, one can observe that the overall classification accuracy of the proposed method (99.68%) was higher than all the other works of literature.
- On the other hand, results from literature adopting various machine learning classifiers for diagnosing faults in PVM were compared with the proposed method as presented in Fig. 11. One can observe that the proposed method with random forest classifier outperforms all other classifiers with a classification accuracy of 99.68%. The only classifier to achieve a classification accuracy closer to the proposed method was kNN with a classification accuracy of 98.85%. Based on the obtained results, one can suggest that the proposed method can be adopted for real time application of PVM fault diagnosis.

6. Conclusion

In this experimental study, we have proposed an ensemble-based deep neural network (DNN) model for autonomous detection of visual faults such as glass breakage, burn marks, snail trail, and discoloration, delamination on various PV modules. We have evaluated the performance of the proposed ensemble-based DNN model in classifying different visual faults in PV modules. In order to train the model, an image dataset of PVM was prepared using an RGB camera mounted on DJI Mavic 2 Zoom. Subsequently, the proposed ensemble-based DNN model was applied for a feature fusion strategy by combining features of various advanced segmentation techniques, including GLCM, FFT, GLDM, DWT, and texture and performed classification using a random forest classifier. A total number of 252 features were extracted and used in the classification process. The performance of the proposed ensemble-based DNN model was assessed using the training progress, ROC and confusion matrices. We have obtained an accuracy of 99.68% for the proposed model.

Furthermore, the results of the designed network were compared with several other pre-trained deep learning models and multiple machine learning classifiers to demonstrate the superior performance of our proposed model. The functionality of the proposed ensemble-based DNN model has shown that it consumed less computation time and required minimal hardware, which makes it feasible and cost-efficient for real-time application. Thus, the ensemble-based DNN model with random forest classifiers can be credibly adopted to diagnose PVM fault conditions in real-time. The proposed model is compatible with all commercially available UAVs and can be applied in their embedded control units for aerial fault detection. The outcomes of the present study led to detecting the failures on time in PV strings, maximizing the energy yield generated by the PV system. As a future direction, multiple feature extraction strategies can be adopted, and ensemble techniques can be applied to reduce the dimensional complexity of images. On-board deployment of a fault diagnosis system is a viable option and prospect for diagnosing PVM faults. Moreover, we will develop the proposed model to detect other faults which can be identified by infrared (IR) thermography and electroluminescent (EL) techniques.

CRediT authorship contribution statement

S. Naveen Venkatesh: Conceptualization, Data curation, Formal analysis, Investigation, Methodology, Software, Validation, Visualization, Role/Writing – original draft. **B. Rebecca Jeyavadhanam:** Conceptualization, Data curation, Formal analysis, Funding acquisition, Investigation, Methodology, Resources, Supervision, Validation, Role/Writing – review & editing. **A.M. Moradi Sizkouhi:** Investigation, Role/Writing – review & editing. **S.M. Esmailifar:** Investigation, Role/Writing – review & editing. **M. Aghaei:** Conceptualization, Data curation, Formal analysis, Funding acquisition, Investigation, Methodology, Supervision, Validation, Role/Writing – review & editing. **V. Sugumaran:** Conceptualization, Data curation, Formal analysis, Funding acquisition, Investigation, Methodology, Resources, Supervision, Validation, Role/Writing – review & editing.

Declaration of competing interest

The authors declare that they have no known competing financial interests or personal relationships that could have appeared to influence the work reported in this paper.

Data availability

The data that has been used is confidential.

References

Abbas, M., Zhang, D., 2021. A smart fault detection approach for PV modules using Adaptive Neuro-Fuzzy Inference framework. Energy Reports 7, 2962–2975. http://dx.doi.org/10.1016/j.egyr.2021.04.059.

Aboagye, B., Gyamfi, S., Ofosu, E.A., Djordjevic, S., 2021. Degradation analysis of installed solar photovoltaic (PV) modules under outdoor conditions in Ghana. Energy Rep. 7, 6921–6931. http://dx.doi.org/10.1016/j.egyr.2021.10.046.

Aghaei, M., Korevaar, M., Babal, P., Ziar, H., 2022. Bifacial Photovoltaic Technology: Recent Advancements, Simulation and Performance Measurement.

Akram, M.W., Li, G., Jin, Y., Chen, X., Zhu, C., Ahmad, A., 2020. Automatic detection of photovoltaic module defects in infrared images with isolated and develop-model transfer deep learning. Sol. Energy 198, 175–186. http://dx.doi.org/10.1016/j.solener.2020.01.055.

Akram, M.W., Li, G., Jin, Y., Chen, X., Zhu, C., Zhao, X., Khaliq, A., Faheem, M., Ahmad, A., 2019. CNN based automatic detection of photovoltaic cell defects in electroluminescence images. Energy 189, 116319. http://dx.doi.org/10.1016/j.energy.2019.116319.

Alvarenga, A.V., Pereira, W.C.A., Infantosi, A.F.C., Azevedo, C.M., 2007. Complexity curve and grey level co-occurrence matrix in the texture evaluation of breast tumor on ultrasound images. Med. Phys. 34, 379–387. http://dx.doi.org/10.1118/1.2401039.

Aziz, F., Ul Haq, A., Ahmad, S., Mahmoud, Y., Jalal, M., Ali, U., 2020. A novel convolutional neural network-based approach for fault classification in photovoltaic arrays. IEEE Access 8, 41889–41904. http://dx.doi.org/10.1109/ACCESS.2020.2977116.

Bentley, P.M., McDonnell, J.T.E., 1994. Wavelet transforms: An introduction. Electron. Commun. Eng. J. 6, 175–186. http://dx.doi.org/10.1049/ecej:19940401.

Bommes, L., Pickel, T., Buerhop-Lutz, C., Hauch, J., Brabec, C., Peters, I.M., 2021. Computer vision tool for detection, mapping, and fault classification of photovoltaics modules in aerial IR videos. Prog. Photovoltaics Res. Appl. 29, 1236–1251. http://dx.doi.org/10.1002/pip.3448.

Bouraiou, A., Hamouda, M., Chaker, A., Neçaibia, A., Mostefaoui, M., Boutasseta, N., Ziane, A., Dabou, R., Sahouane, N., Lachtar, S., 2018. Experimental investigation of observed defects in crystalline silicon PV modules under outdoor hot dry climatic conditions in Algeria. Sol. Energy 159, 475–487. http://dx.doi.org/10.1016/j.solener.2017.11.018.

Chandel, S.S., Nagaraju Naik, M., Sharma, V., Chandel, R., 2015. Degradation analysis of 28 year field exposed mono-c-si photovoltaic modules of a direct coupled solar water pumping system in western Himalayan region of India. Renew. Energy 78, 193–202. http://dx.doi.org/10.1016/j.renene.2015.01.015.

Chen, Z., Han, F., Wu, L., Yu, J., Cheng, S., Lin, P., Chen, H., 2018. Random forest based intelligent fault diagnosis for PV arrays using array voltage and string currents. Energy Convers. Manag. 178, 250–264. http://dx.doi.org/10.1016/j.enconman.2018.10.040.

D'Adamo, I., Gastaldi, M., Morone, P., 2020. The post COVID-19 green recovery in practice: Assessing the profitability of a policy proposal on residential photovoltaic plants. Energy Policy 147, 111910. http://dx.doi.org/10.1016/j.enpol.2020.111910.

De Guia, J.D., Concepcion, R.S., Calinao, H.A., Lauguico, S.C., Dadios, E.P., Vicerra, R.R.P., 2020. Application of ensemble learning with mean shift clustering for output profile classification and anomaly detection in energy production of grid-tied photovoltaic system. In: ICITEE 2020 - Proc. 12th Int. Conf. Inf. Technol. Electr. Eng. pp. 286–291. http://dx.doi.org/10.1109/ICITEE49829.2020.9271699.

Dhibi, K., Mansouri, M., Bouzrara, K., Nounou, H., Nounou, M., 2021. An enhanced ensemble learning-based fault detection and diagnosis for grid-connected PV systems. IEEE Access 9, 155622–155633. http://dx.doi.org/10.1109/ACCESS.2021.3128749.

Dolara, A., Lazaroiu, G.C., Leva, S., Manzolini, G., Votta, L., 2016. Snail trails and cell microcrack impact on PV module maximum power and energy production. IEEE J. Photovoltaics 6, 1269–1277. http://dx.doi.org/10.1109/JPHOTOV.2016.2576682.

Eskandari, A., Milimonfared, J., Aghaei, M., 2020a. Line-line fault detection and classification for photovoltaic systems using ensemble learning model based on I-V characteristics. Sol. Energy 211, 354–365. http://dx.doi.org/10.1016/j.solener.2020.09.071.

Eskandari, A., Milimonfared, J., Aghaei, M., 2020b. Fault detection and classification for photovoltaic systems based on hierarchical classification and machine learning technique. IEEE Trans. Ind. Electron http://dx.doi.org/10.1109/TIE.2020.3047066.

Fonseca Alves, R.H., Deus Júnior, G.A. de, Marra, E.G., Lemos, R.P., 2021. Automatic fault classification in photovoltaic modules using convolutional neural networks. Renew. Energy 179, 502–516. http://dx.doi.org/10.1016/j.renene.2021.07.070.

Grimaccia, F., Leva, S., Dolara, A., Aghaei, M., 2017. Survey on PV modules' common faults after an o & m flight extensive campaign over different plants in Italy. IEEE J. Photovoltaics 7, 810–816.

Grimaccia, F., Leva, S., Niccolai, A., Cantoro, G., 2018. Assessment of PV plant monitoring system by means of unmanned aerial vehicles. In: Proc. - 2018 IEEE Int. Conf. Environ. Electr. Eng. 2018 IEEE Ind. Commer. Power Syst. Eur. EEEIC/I CPS Eur, Vol. 2018. pp. 1–6. http://dx.doi.org/10.1109/EEEIC.2018.8494532.

Han, H., Dong, X., Li, B., Yan, H., Verlinden, P.J., Liu, J., Huang, J., Liang, Z., Shen, H., 2018. Degradation analysis of crystalline silicon photovoltaic modules exposed over 30 years in hot-humid climate in China. Sol. Energy 170, 510–519. http://dx.doi.org/10.1016/j.solener.2018.05.027.

Harrou, F., Taghezouit, B., Sun, Y., 2019. Robust and flexible strategy for fault detection in grid-connected photovoltaic systems. Energy Convers. Manag. 180, 1153–1166. http://dx.doi.org/10.1016/j.enconman.2018.11.022.

Hong, Y.Y., Pula, R.A., 2022. Methods of photovoltaic fault detection and classification: A review. Energy Rep. 8, 5898–5929. http://dx.doi.org/10.1016/j.egyr.2022.04.043.

Kettle, J., Aghaei, M., Ahmad, S., Fairbrother, A., Irvine, S., Jacobsson, T.J., Kazim, S., Kazukauskas, V., Lamb, D., Lobato, K., 2022. Review of technology specific degradation in c-Si, CdTe, CIGS, dye sensitised, organic and perovskite solar cells in photovoltaic modules; understanding how reliability improvements in mature technologies can enhance emerging technologies. Prog. Photovoltaics.

Kim, K.W., Hong, H.G., Nam, G.P., Park, K.R., 2017. A study of deep CNN-based classification of open and closed eyes using a visible light camera sensor. Sensors (Switzerland) 17, http://dx.doi.org/10.3390/s17071534.

Kirsten Vidal de Oliveira, A., Aghaei, M., Rüther, R., 2020. Aerial infrared thermography for low-cost and fast fault detection in utility-scale PV power plants. Sol. Energy http://dx.doi.org/10.1016/j.solener.2020.09.066.

Köntges, M., Kurtz, S., Packard, C., Jahn, U., Berger, K.A., Kato, K., Friesen, T., Liu, H., Van Iseghem, M., 2014. IEA-PVPS T13-01 2014 review of failures of photovoltaic modules final.

Korkmaz, D., Acikgoz, H., 2022. An efficient fault classification method in solar photovoltaic modules using transfer learning and multi-scale convolutional neural network. Eng. Appl. Artif. Intell 113, 104959. http://dx.doi.org/10.1016/j.engappai.2022.104959.

Krishnaswamy Rangarajan, A., Purushothaman, R., 2020. Disease classification in eggplant using pre-trained VGG16 and MSVM. Sci. Rep. 10, 1–11. http://dx.doi.org/10.1038/s41598-020-59108-x.

Krizhevsky, A., Sutskever, I., Hinton, G.E., 2017. ImageNet classification with deep convolutional neural networks. Commun. ACM 60, 84–90. http://dx.doi.org/10.1145/3065386.

Leva, S., Aghaei, M., Grimaccia, F., 2015. PV power plant inspection by UAS: Correlation between altitude and detection of defects on PV modules. In: 2015 IEEE 15th International Conference on Environment and Electrical Engineering, EEEIC 2015 - Conference Proceedings. http://dx.doi.org/10.1109/EEEIC.2015.7165466.

Li, X., Yang, Q., Chen, Z., Luo, X., Yan, W., 2017. Visible defects detection based on UAV-based inspection in large-scale photovoltaic systems. IET Renew. Power Gener. 11, 1234–1244. http://dx.doi.org/10.1049/iet-rpg.2017.0001.

Li, X., Yang, Q., Lou, Z., Yan, W., 2019. Deep learning based module defect analysis for large-scale photovoltaic farms. IEEE Trans. Energy Convers. 34, 520–529. http://dx.doi.org/10.1109/TEC.2018.2873358.

Li, X., Yang, Q., Wang, J., Chen, Z., Yan, W., 2018. Intelligent fault pattern recognition of aerial photovoltaic module images based on deep learning technique. In: IMCIC 2018-9th Int. Multi-Conference Complexity, Informatics Cybern. Proc, vol. 1. pp. 22–27.

Liang, M., Cao, P., Tang, J., 2021. Rolling bearing fault diagnosis based on feature fusion with parallel convolutional neural network. Int. J. Adv. Manuf. Technol. 112, 819–831. http://dx.doi.org/10.1007/s00170-020-06401-8.

Lu, X., Lin, P., Cheng, S., Lin, Y., Chen, Z., Wu, L., Zheng, Q., 2019. Fault diagnosis for photovoltaic array based on convolutional neural network and electrical time series graph. Energy Convers. Manag. 196, 950–965. http://dx.doi.org/10.1016/j.enconman.2019.06.062.

Luo, Z., Cheng, S.Y., Zheng, Q.Y., 2019. Corrigendum: GAN-based augmentation for improving CNN performance of classification of defective photovoltaic module cells in electroluminescence images (IOP conf. Ser.: Earth environ. Sci. 354 012106). IOP Conf. Ser. Earth Environ. Sci. 354, 012132. http://dx.doi.org/10.1088/1755-1315/354/1/012132.

Madeti, S.R., Singh, S.N., 2018. Modeling of PV system based on experimental data for fault detection using kNN method. Sol. Energy 173, 139–151. http://dx.doi.org/10.1016/j.solener.2018.07.038.

Manjunath, B.S., Haley, G.M., Ma, W.Y., Newsam, S.D., 2005. Multiband techniques for texture classification and segmentation. In: Handbook of Image and Video Processing, Second ed. Elsevier Inc., http://dx.doi.org/10.1016/B978-012119792-6/50091-7.

Manno, D., Cipriani, G., Ciulla, G., Di Dio, V., Guarino, S., Lo Brano, V., 2021. Deep learning strategies for automatic fault diagnosis in photovoltaic systems by thermographic images. Energy Convers. Manag. 241, http://dx.doi.org/10.1016/j.enconman.2021.114315.

Márquez, F.P.G., Papaelias, M., 2019. An overview of wind turbine maintenance management. In: Non-Destructive Testing and Condition Monitoring Techniques for Renewable Energy Industrial Assets. Elsevier Ltd., http://dx.doi.org/10.1016/B978-0-08-101094-5.00003-4.

Moradi Sizkouhi, A., Aghaei, M., Esmailifar, S.M., 2021. A deep convolutional encoder-decoder architecture for autonomous fault detection of PV plants using multi-copters. Sol. Energy 223, 217–228. http://dx.doi.org/10.1016/j.solener.2021.05.029.

Naveen Venkatesh, S., Sugumaran, V., 2022. Machine vision based fault diagnosis of photovoltaic modules using lazy learning approach. Meas. J. Int. Meas. Confed. 191, 110786. http://dx.doi.org/10.1016/j.measurement.2022.110786.

Niazi, K.A.K., Akhtar, W., Khan, H.A., Yang, Y., Athar, S., 2019. Hotspot diagnosis for solar photovoltaic modules using a naive Bayes classifier. Sol. Energy 190, 34–43. http://dx.doi.org/10.1016/j.solener.2019.07.063.

Niccolai, A., Gandelli, A., Grimaccia, F., Zich, R., Leva, S., 2019. Overview on photovoltaic inspections procedure by means of unmanned aerial vehicles. In: 2019 IEEE Milan PowerTech. IEEE, pp. 1–6. http://dx.doi.org/10.1109/PTC.2019.8810987.

Pan, L., Zhao, L., Song, A., She, S., Wang, S., 2021. Research on gear fault diagnosis based on feature fusion optimization and improved two hidden layer extreme learning machine. Meas. J. Int. Meas. Confed. 177, 109317. http://dx.doi.org/10.1016/j.measurement.2021.109317.

Perveen, G., Rizwan, M., Goel, N., Anand, P., 2020. Artificial neural network models for global solar energy and photovoltaic power forecasting over India. Energy Sources, Part A Recover. Util. Environ. Eff. 00, 1–26. http://dx.doi.org/10.1080/15567036.2020.1826017.

Pierdicca, R., Malinverni, E.S.S., Piccinini, F., Paolanti, M., Felicetti, A., Zingaretti, P., 2018. Deep convolutional neural network for automatic detection of damaged photovoltaic cells. In: ISPRS - Int. Arch. Photogramm. Remote Sens. Spat. Inf. Sci. XLII–2. pp. 893–900. http://dx.doi.org/10.5194/isprs-archives-XLII-2-893-2018.

S, N.V., Sugumaran, V., 2020. Fault diagnosis of visual faults in photovoltaic modules: A review. Int. J. Green Energy http://dx.doi.org/10.1080/15435075.2020.1825443.

Sánchez-Friera, P., Piliougine, M., Peláez, J., Carretero, J., De Cardona, M.S., 2011. Analysis of degradation mechanisms of crystalline silicon PV modules after 12 years of operation in southern europe. Prog. Photovoltaics Res. Appl. 19, 658–666. http://dx.doi.org/10.1002/pip.1083.

Shao, H., Jiang, H., Wang, F., Zhao, H., 2017. An enhancement deep feature fusion method for rotating machinery fault diagnosis. Knowl.-Based Syst. 119, 200–220. http://dx.doi.org/10.1016/j.knosys.2016.12.012.

Sizkouhi, A.M.M., Esmailifar, S.M., Aghaei, M., Karimkhani, M., 2022. RoboPV: An integrated software package for autonomous aerial monitoring of large scale PV plants. Energy Convers. Manag. 254, 115217.

Sizkouhi, A.M.M., Esmailifar, S.M., Aghaei, M., Vidal de Oliveira, A.K., Rüther, R., 2019. Autonomous path planning by unmanned aerial vehicle (UAV) for precise monitoring of large-scale PV plants. In: 46th IEEE PVSC.

Sridharan, N.V., Sugumaran, V., 2021. Visual fault detection in photovoltaic modules using decision tree algorithms with deep learning features. Energy Sources Part A Recov. Util. Environ. Eff. 00, 1–17. http://dx.doi.org/10.1080/15567036.2021.2020379.

Sun, T., Xing, H., Cao, S., Zhang, Y., Fan, S., Liu, P., 2022. A novel detection method for hot spots of photovoltaic (PV) panels using improved anchors and prediction heads of YOLOv5 network. Energy Reports 8, 1219–1229. http://dx.doi.org/10.1016/j.egyr.2022.08.130.

Tang, W., Yang, Q., Xiong, K., Yan, W., 2020. Deep learning based automatic defect identification of photovoltaic module using electroluminescence images. Sol. Energy 201, 453–460. http://dx.doi.org/10.1016/j.solener.2020.03.049.

Tao, X., Zhang, D., Ma, W., Liu, X., Xu, De., 2018. Automatic metallic surface defect detection and recognition with convolutional neural networks. Appl. Sci. 8, 1–15. http://dx.doi.org/10.3390/app8091575.

Tsanakas, J.A., Chrysostomou, D., Botsaris, P.N., Gasteratos, A., 2015. Fault diagnosis of photovoltaic modules through image processing and canny edge detection on field thermographic measurements. Int. J. Sustain. Energy 34, 351–372. http://dx.doi.org/10.1080/14786451.2013.826223.

Tsanakas, J.A., Ha, L.D., Al Shakarchi, F., 2017. Advanced inspection of photovoltaic installations by aerial triangulation and terrestrial georeferencing of thermal/visual imagery. Renew. Energy 102, 224–233. http://dx.doi.org/10.1016/j.renene.2016.10.046.

Venkatesh, S.N., Sugumaran, V., 2021. A combined approach of convolutional neural networks and machine learning for visual fault classification in photovoltaic modules. Proc. Inst. Mech. Eng. Part O J. Risk Reliab. http://dx.doi.org/10.1177/1748006X211020305.

Vidal de Oliveira, A.K., Mohammedreza, A., Rüther, R., 2019. Automatic fault detection of photovoltaic array by convolutional neural. In: 36th Eur. Photovolt. Sol. Energy Conf. Exhib. pp. 1302–1307.

Wang, X., Yang, W., Qin, B., Wei, K., Ma, Y., Zhang, D., 2022. Intelligent monitoring of photovoltaic panels based on infrared detection. Energy Rep. 8, 5005–5015. http://dx.doi.org/10.1016/j.egyr.2022.03.173.

Wen, L., Li, X., Gao, L., 2019. A transfer convolutional neural network for fault diagnosis based on ResNet-50. Neural Comput. Appl. 0123456789. http://dx.doi.org/10.1007/s00521-019-04097-w.

Ying, Z., Li, M., Tong, W., Haiyong, C., 2019. Automatic detection of photovoltaic module cells using multi-channel convolutional neural network. In: Proc. 2018 Chinese Autom. Congr. CAC, Vol. 2018. pp. 3571–3576. http://dx.doi.org/10.1109/CAC.2018.8623258.

Zsiborács, H., Zentkó, L., Pintér, G., Vincze, A., Baranyai, N.H., 2021. Assessing shading losses of photovoltaic power plants based on string data. Energy Rep. 7, 3400–3409. http://dx.doi.org/10.1016/j.egyr.2021.05.038.